A LOW-MASS H₂ COMPONENT TO THE AU MICROSCOPII CIRCUMSTELLAR DISK[1]

KEVIN FRANCE,[2] AKI ROBERGE,[3] ROXANA E. LUPU,[4] SETH REDFIELD,[5,6] AND PAUL D. FELDMAN[4]

ABSTRACT

We present a determination of the molecular gas mass in the AU Microscopii circumstellar disk. Direct detection of a gas component to the AU Mic disk has proven elusive, with upper limits derived from ultraviolet absorption line and submillimeter CO emission studies. Fluorescent emission lines of H_2, pumped by the O VI $\lambda 1032$ resonance line through the $C–X\,(1–1)\,Q(3)\,\lambda 1031.87$ Å transition, are detected by the *Far Ultraviolet Spectroscopic Explorer*. These lines are used to derive the H_2 column density associated with the AU Mic system. The derived column density is in the range $N(H_2) = 1.9 \times 10^{17}$ to 2.8×10^{15} cm^{-2}, roughly 2 orders of magnitude lower than the upper limit inferred from absorption line studies. This range of column densities reflects the range of H_2 excitation temperature consistent with the observations, $T(H_2) = 800–2000$ K, derived from the presence of emission lines excited by O VI in the absence of those excited by Lyα. Within the observational uncertainties, the data are consistent with the H_2 gas residing in the disk. The inferred $N(H_2)$ range corresponds to H_2-to-dust ratios of $\lesssim \frac{1}{30}$:1 and a total $M(H_2) = 4.0 \times 10^{-4}$ to $5.8 \times 10^{-6}\,M_\oplus$. We use these results to predict the intensity of the associated rovibrational emission lines of H_2 at infrared wavelengths covered by ground-based instruments, *HST* NICMOS, and the *Spitzer* IRS.

Subject headings: circumstellar matter — planetary systems: protoplanetary disks — stars: individual (AU Microscopii, HD 197481) — ultraviolet: stars

Online material: color figure

1. INTRODUCTION

Circumstellar (CS) disks around young main-sequence stars appear to be in transition between massive, gas-rich protoplanetary disks and low-mass, gas-poor planetary systems. Surveys for CS disks in young stellar clusters suggest that gas-rich protoplanetary disks dissipate on timescales of ~1–10 Myr (Bally et al. 1998; Haisch et al. 2001). For solar-type stars, the timescale for gas dissipation is roughly equal to the theoretical time required for gas giant planet formation by the standard core-accretion method (e.g., Hubickyj et al. 2005). For low-mass M stars, on the other hand, the time required to form giant planets by core accretion is much longer than it is around solar-type stars, and may be longer than the typical gas disk lifetimes (Laughlin et al. 2004). Consequently, observations of the gas component in the disks of low- and intermediate-mass main-sequence stars undergoing the transition from gas-rich protoplanetary disk to gas-poor debris disk are important for constraining giant planet formation scenarios.

AU Microscopii is a nearby ($d \approx 10$ pc) M1 star surrounded by an edge-on (inclination $1°–3°$) dust disk (Kalas et al. 2004; Krist et al. 2005). The star is a very active flare star, and the majority of AU Mic studies prior to imaging of its disk focused on the stellar activity (Redfield et al. 2002 and references therein). AU Mic is a member of the β Pictoris moving group, indicating an age of $t_{\rm AU\,Mic} = 12^{+8}_{-4}$ Myr (Zuckerman et al. 2001). The star β Pic (A5 V) itself has a well-studied edge-on debris disk (Roberge et al. 2000; Lecavelier des Etangs et al. 2001). These two stars al-

low us to examine possible differences between disks of the same age around stars of very different mass.

Liu et al. (2004) measured the 850 μm dust emission from the AU Mic disk and inferred a total mass of 0.011 $M_\oplus$ at $T_{\rm dust} = 40$ K. No submillimeter CO emission was detected, implying a low CS gas mass; however, this upper limit was not very stringent. A much lower upper limit on the column density of molecular gas was determined using far-UV H_2 absorption spectroscopy (Roberge et al. 2005). This study indicated that the H_2-to-dust ratio in the disk is less than about 6 : 1, dramatically depleted from the canonical interstellar ratio of 100 : 1. Roberge et al. (2005) mentioned that there was an indication of weak H_2 absorption at a column density at least an order of magnitude below their upper limit. They also noted the presence of very weak fluorescent H_2 emission lines in the far-UV spectra, which had been seen in previous work (Redfield et al. 2002).

An M star has insufficient continuum flux to excite ("pump") far-UV fluorescent emission. In general, only stars of type ~B3 and earlier have the necessary spectral energy distribution ($\lambda \leq 1110$ Å) to produce detectable levels of continuum pumped UV fluorescence (France 2005). However, pre-main-sequence and low-mass dwarf stars show high-temperature emission lines arising in their chromospheric and coronal regions (Linsky & Wood 1994; Wood et al. 1997; Redfield et al. 2002, 2003). These stellar emission lines can coincide in wavelength with transitions of H_2, providing the necessary flux to excite detectable fluorescence when CS material is present. Line pumped H_2 fluorescence has been observed from a variety of environments, including T Tauri disks (Valenti et al. 2000; Wilkinson et al. 2002; Herczeg et al. 2006), sunspots (Jordan et al. 1977), solar system comet comae (Feldman et al. 2002), and recently from planetary nebulae (Lupu et al. 2006).

Here we present a detailed description and analysis of the fluorescent H_2 emission lines in *Far Ultraviolet Spectroscopic Explorer* (*FUSE*) spectra of AU Mic. The majority of line pumped fluorescence studies have focused on H_2 excitation by Lyα emission (Shull 1978; Black & van Dishoeck 1987). However, in the

---

[2] Canadian Institute for Theoretical Astrophysics, University of Toronto, 60 St. George Street, Toronto, ON M5S 3H8; france@cita.utoronto.ca.

[3] Exoplanets and Stellar Astrophysics Laboratory, NASA Goddard Space Flight Center, Greenbelt, MD 20771; akir@milkyway.gsfc.nasa.gov.

[4] Department of Physics and Astronomy, Johns Hopkins University, Baltimore, MD 21218; roxana@pha.jhu.edu, pdf@pha.jhu.edu.

[5] Department of Astronomy, University of Texas, Austin, TX 78712; sredfield@astro.as.utexas.edu.

[6] Hubble Fellow.
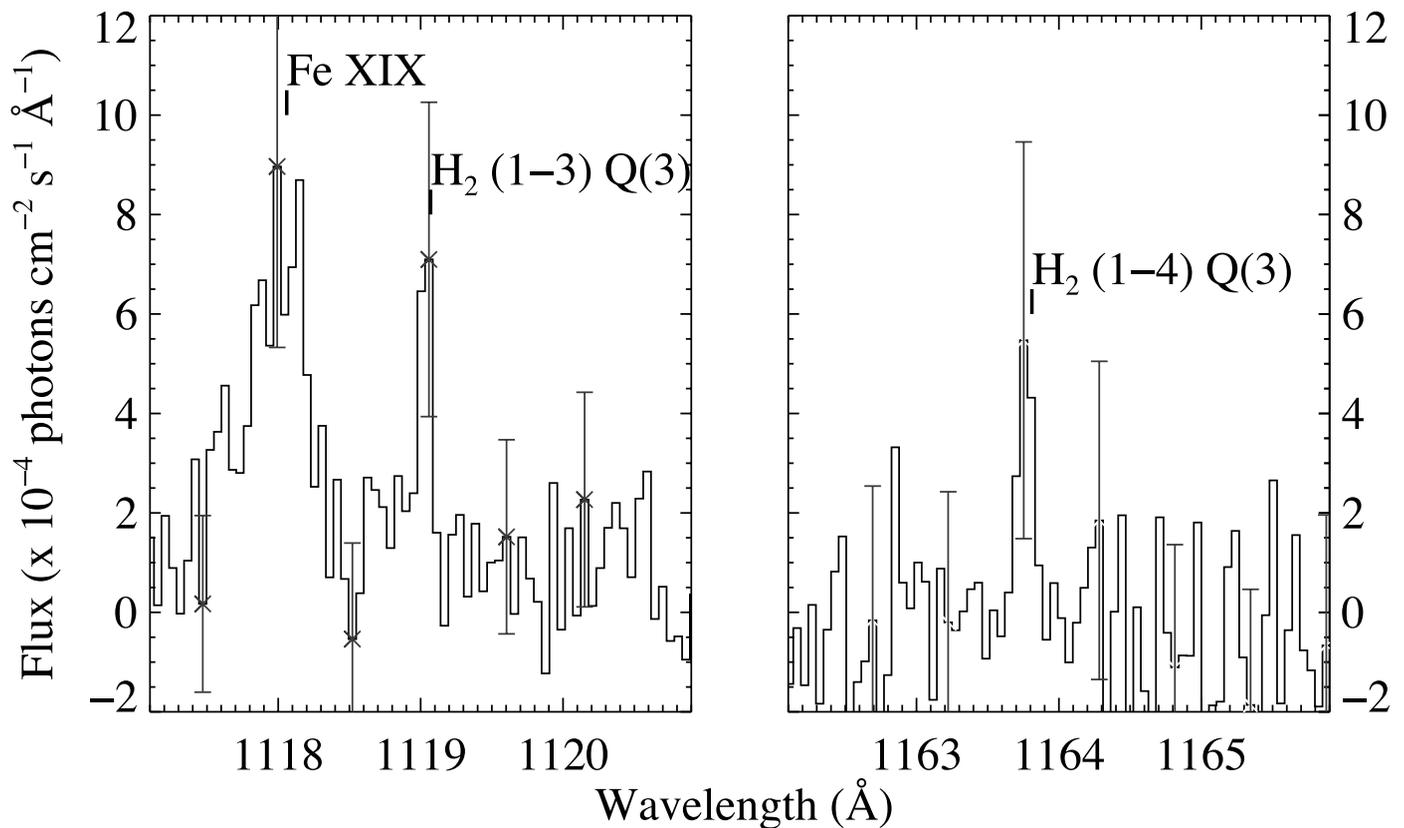
Fɪɢ. 1.—*FUSE* LiF 1B data for the *C–X* (1–3) *Q*(3) λ1119.08 Å and (1–4) *Q*(3) λ1163.81 Å emission lines. The broad feature in the left panel is coronal Fe xɪx (Redfield et al. 2002, 2003). For display, measurement uncertainties on the flux calibration are shown as the error bars on the crosses. [*See the electronic edition of the Journal for a color version of this figure.*]

case of AU Mic, we show that the observed H_2 emission lines are pumped by the O vɪ λ1032 stellar emission line, which is an important excitation source in some situations (Wilkinson et al. 2002; Redfield et al. 2002; Herczeg et al. 2006). In § 2 of this paper, we briefly describe the observations and the characteristics of the detected fluorescent H_2 emission lines. In § 3, we calculate the total fluorescent H_2 flux, constrain the H_2 temperature, and determine the total column density of absorbing H_2. Our estimation of the total mass of H_2 gas in the AU Mic system appears in § 4. This section also contains a discussion of the H_2 heating and its implications for the gas location. A comparison between the observed AU Mic and β Pic disk properties is given in § 5, and predictions for the near- and mid-IR H_2 emission line fluxes of AU Mic appear in § 6. Our results are summarized in § 7.

2. *FUSE* OBSERVATIONS AND H_2 LINE IDENTIFICATION

FUSE performs medium-resolution ($\Delta v \approx 15$ km s^{-1}) spectroscopy in the far-UV bandpass (905–1187 Å). The *FUSE* observatory is described in Moos et al. (2000), and on-orbit performance characteristics are given in Sahnow et al. (2000). AU Mic was observed with *FUSE* early in the mission as part of the "cool stars" programs P118 (2000 August 26, exposure time 17.3 ks) and P218 (2001 October 10, exposure time 26.5 ks). These observations are described in Redfield et al. (2002). These data were acquired in TTAG mode through the 30″ × 30″ LWRS aperture. The data have been reprocessed with the CalFUSE pipeline, version 2.4.0. Data taken during periods of stellar flare activity were excluded (Roberge et al. 2005). The fluorescent emission lines studied here fall on the LiF 2A (1087–1179 Å) and LiF 1B (1092–

1187 Å) detector segments. Archival *HST* Space Telescope Imaging Spectrograph (STIS) spectra of the chromospheric C ɪɪɪ λ1176 multiplet were used to establish the wavelength calibration of the *FUSE* LiF 1B channel (Roberge et al. 2005). Due to a lower background in the (1–3) *Q*(3) λ1119.08 Å region, we present the LiF 1B data here.

The H_2 emission lines observed in the LiF 1B channel are shown in Figure 1. The *C–X* (1–3) *Q*(3) λ1119.077 Å and *C–X* (1–4) *Q*(3) λ1163.807 Å transitions are shown in the left and right panels, respectively. These lines are excited by absorption in the *C–X* (1–1) *Q*(3) λ1031.87 Å line, which is coincident with the strong stellar O vɪ λ1032 emission line. A description of the electronic excitation of H_2 and the molecular notation is given in Shull & Beckwith (1982). The (1–3) and (1–4) lines are expected to be the brightest ones in the O vɪ pumped fluorescent cascade (Abgrall et al. 1993b). A Gaussian least-squares fitting routine was used to derive the line strength, width, velocity, and detection levels. The lines were marginally resolved and displayed a slight blueshift with respect to the stellar velocity ($v_* = -4.98 \pm 0.02$ km s^{-1}). The (1–3) line was detected at 2.6 σ with an integrated line strength of $I_{(1-3)} = (1.61 \pm 0.62) \times 10^{-15}$ ergs s^{-1} cm^{-2} [$(9.07 \pm 3.49) \times 10^{-5}$ photons s^{-1} cm^{-2}] in the 30″ × 30″ aperture. Its velocity[7] was $v_{(1-3)} = -12.0 \pm 2.8$ km s^{-1} with a FWHM$_{(1-3)} = 26 \pm 7$ km s^{-1} and a peak observed flux of 12.5×10^{-15} ergs s^{-1} cm^{-2} Å^{-1}. The (1–4) line was detected at 1.9 σ with an integrated line strength of $I_{(1-4)} = (1.48 \pm 0.76) \times 10^{-15}$ ergs s^{-1} cm^{-2} [$(8.67 \pm 4.45) \times 10^{-5}$ photons s^{-1} cm^{-2}]

---

[7] A detailed description of the *FUSE* wavelength calibration can be found at http://fuse.pha.jhu.edu /analysis/calfuse.html.

Line Parameter	H₂ (1–3) Q(3)	H₂ (1–4) Q(3)
λ_o (Å)	1119.077	1163.807
λ_{obs} (Å)	1119.03	1163.72
v (km s⁻¹)	-12.0 ± 2.8	-22.3 ± 4.1
FWHM (km s⁻¹)	26 ± 7	35 ± 9
I_{ik} [a]	$(9.07 \pm 3.49) \times 10^{-5}$	$(8.67 \pm 4.45) \times 10^{-5}$
F_{peak} [b]	7.0×10^{-4}	5.6×10^{-4}

[a] Integrated line strength in units of photons cm⁻² s⁻¹.
[b] Peak line strength in units of photons cm⁻² s⁻¹ Å⁻¹.

over the same area. The (1−4) emission line was at a velocity of $v_{(1-4)} = -22.3 \pm 4.1$ km s⁻¹ with a FWHM$_{(1-4)} = 35 \pm 9$ km s⁻¹ and a peak observed flux of 9.5×10^{-15} ergs s⁻¹ cm⁻² Å⁻¹. These findings are summarized in Table 1.

The observed ratios of the detected emission lines (R_{34}) are consistent with the theoretical branching ratios within the 1 σ uncertainty [R_{34}(observed) = 1.05 ± 0.41 vs. R_{34}(predicted) = 0.76]. The difference between the observed and theoretical ratios may be due to suppression of the (1−4) 1163.81 Å line by "the worm" seen in *FUSE* spectra from the LiF 1B channel.[8] The line ratios derived from the LiF 2A channel are somewhat closer to the theoretical value, although with larger uncertainties (R_{34} observed in LiF 2A = 0.89 ± 0.55). The discrepancy is not significant within the observational uncertainties and does not affect the results presented in §§ 3 and 4. The only other H₂ emission line with a comparable branching ratio in the *FUSE* bandpass is the $C-X$ (1−0) Q(3) λ989.73 Å transition. This wavelength region has a lower instrumental effective area and is dominated by a combination of geocoronal O I and stellar N III lines. No H₂ emission from $C-X$ (1−0) Q(3) was observed.

The H₂ $C-X$ (1−5) Q(3) λ1208.93 Å and $C-X$ (1−6) Q(3) λ1254.11 Å emission lines located in the STIS bandpass have branching ratios relative to (1−3) 1119.08 Å (R_{53} and R_{63}) of roughly 0.6 and 0.1, respectively. Emission lines were detected at these wavelengths at the 2–3 σ level. Their velocities and line strengths are consistent with the observed H₂ emission lines in the *FUSE* spectra. We focus on the lines in the *FUSE* bandpass for the remainder of the paper, but we note that the detection of additional H₂ fluorescent emission lines with an independent instrument makes the conclusions presented in §§ 3 and 4 more robust.

3. ANALYSIS AND RESULTS

3.1. *Total Emitted* H₂ *Flux*

Using the measured H₂ emission line fluxes, we can calculate the total fluorescent output from the O VI pumped cascade. The total emitted flux out of the electrovibrational state (n', v', J'), $\sum_j I_{ij}$, is given by

$$\sum_j I_{ij} = I_{ik} \left(\frac{A_{ik}}{\sum_l A_{il}} \right)^{-1} (1 - \xi_i)^{-1}, \qquad (1)$$

where i refers to the upper state (n', v', J'). The indices j, k, and l refer to the lower states (n'', v'', J''). Here I_{ik} is the measured flux of the *FUSE* band lines (in photons s⁻¹ cm⁻²). The ratios of individual to total Einstein A-values (Abgrall et al. 1993b) are

[8] More information about "the worm" can be found on the *FUSE* data analysis page at http://fuse.pha.jhu.edu/analysis/calfuse_wp6.html.

the branching ratios, and ξ_i is a correction for the efficiency of predissociation in the excited electronic state (Liu & Dalgarno 1996). In the case of AU Mic, we are concerned with Werner band emission ($n'-n'' = C-X \equiv C^1\Pi_u - X^1\Sigma_g^+$), $v' = 1$, and $v'' = 3$ and 4 for the 1119.08 and 1163.81 Å lines, respectively. The predissociation fraction for the Werner bands is zero ($\xi_C = 0$; Ajello et al. 1984).

By following this procedure, we arrived at the total emitted photon flux, $\sum_j I_{ij}$, derived from the observed (1−3) 1119.08 Å and (1−4) 1163.81 Å emission lines individually [$(4.3 \pm 1.7) \times 10^{-4}$ and $(3.1 \pm 1.6) \times 10^{-4}$ photons s⁻¹ cm⁻² for the (1−3) and (1−4) lines, respectively]. For the determination of the total H₂ column density presented below, we take the average of these values, $\sum_j I_{ij} = (3.7 \pm 2.3) \times 10^{-4}$ photons s⁻¹ cm⁻². The error on the total emitted flux was determined such that both the (1−3) 1119.08 Å and (1−4) 1163.81 Å values are consistent with the mean value; this approach ensures a conservative estimate of the measurement uncertainties.

3.2. *Inferred* H₂ *Column Density*

In order to determine the total column density that is associated with the observed level of emission, we made three assumptions: (1) that fluorescence is the only source of the observed emission, (2) that the stellar O VI λ1032 emission line is the only source of pumping photons, and (3) that the total number of photons is conserved. Assumption 1 seems warranted as H₂ cannot be electronically excited by shocks or collisional processes with other gas or dust particles. In addition, excitation by electron collisions has a distinct far-UV emission signature (Ajello et al. 1982) which is not observed toward AU Mic. As for assumption 2, AU Mic does not emit stellar continuum at wavelengths coincident with the absorbing transitions that produce the fluorescent emission lines, supporting the assumption that the O VI emission line is responsible for the observed excitation. Finally, for assumption 3, detailed calculations of the formation and destruction of molecules in the AU Mic system are beyond the scope of this work; thus, we assumed photon conservation for what follows.

Roberge et al. (2005) modeled the O VI λ1032/λ1038 and C II λ1036/λ1037 stellar emission lines in the *FUSE* data by fitting a combination of narrow and broad Gaussians to each line. The high-excitation ionic lines thought to originate in the chromosphere and transition regions of low-mass dwarf stars are known to be poorly fit by a single Gaussian component (Linsky & Wood 1994; Redfield et al. 2002). The narrow component of the profile has a FWHM$_{narrow} = 44 \pm 6$ km s⁻¹ with a velocity of $v_{narrow} = -4.6 \pm 1.6$ km s⁻¹. This is consistent with the stellar velocity ($v_* = -4.98 \pm 0.02$ km s⁻¹). The broad component has FWHM$_{broad} = 109 \pm 25$ km s⁻¹ with a somewhat redshifted velocity of $v_{broad} = +7.7 \pm 9.3$ km s⁻¹ (Roberge et al. 2005). This two-component model was used as the stellar emission profile to be absorbed by the $C-X$ (1−1) Q(3) λ1031.87 Å transition. The absorption profile was created from an H₂ools optical depth template (McCandliss 2003) with a conservative Doppler parameter $b = 2$ km s⁻¹ (Lecavelier des Etangs et al. 2001). The H₂ools templates are optical depth arrays that can be used to fit arbitrary H₂ column densities for many rovibrational states for b-values from 2 to 20 km s⁻¹ (McCandliss 2003). The stellar emission model was binned to 0.01 Å pixels to match the H₂ools wavelength grid. A grid of column densities was searched to find the minimum difference in the absorbed [I(O VI$_{model}$)−I(O VI$_{model} \times$ H₂ absorption)] and emitted fluxes (the equilibrium condition). This method found N(H₂, n, v, J) = $N_{X,1,3}$ = $3.48^{+2.02}_{-1.48} \times 10^{13}$ cm⁻². The O VI model and H₂ absorption are illustrated in Figure 2.
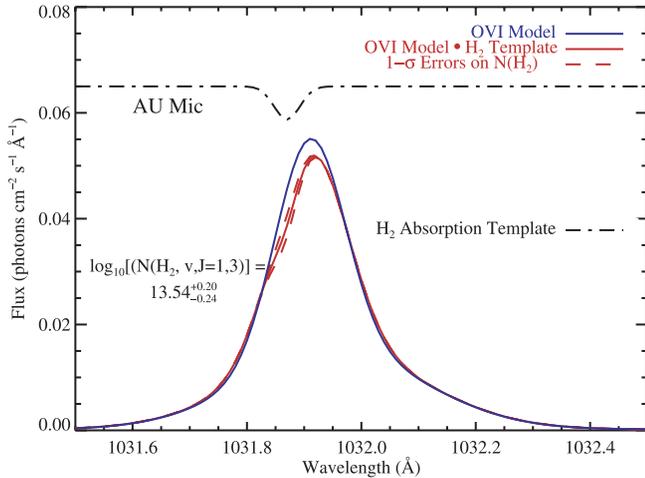
FIG. 2.—Excitation of fluorescent H$_2$ emission lines by stellar O VI emission. The intrinsic stellar O VI $\lambda 1032$ emission model (Roberge et al. 2005) is shown by the solid blue line. The H$_2$ absorption model with a column density in the $(v, J) = (1, 3)$ level of $N_{X,1,3} = 3.48^{+2.02}_{-1.48} \times 10^{13}$ cm^{-2} is shown at the top with the black dot-dashed line; this model has been convolved with the *FUSE* line-spread function. The solid red line shows the stellar emission model times the H$_2$ absorption model; the shape of the stellar emission line is modified by superimposed absorption from the H$_2$ $C-X$ $(1-1)$ $Q(3)$ transition at 1031.87 Å. This absorption line is the excitation channel for the observed fluorescent H$_2$ emission lines shown in Fig. 1. The red dashed lines show total models with absorption columns corresponding to the quoted error ranges on the H$_2$ column density $N_{X,1,3}$.

The total $N(\mathrm{H}_2)$ can be determined from $N_{X,1,3}$ by assuming a Boltzmann distribution and an estimate for the temperature. Liu et al. (2004) assumed that the CO in the AU Mic disk is in thermal equilibrium with the dust at 40 K, and Roberge et al. (2005) consider absorption out of the $v = 0$, $J = 0$, 1 states of H$_2$ assuming that $T(\mathrm{H}_2) \leq 200$ K. To make our own determination of the H$_2$ excitation temperature, we used far-UV H$_2$ fluorescence models (France et al. 2005) to predict the temperature dependence of the H$_2$ emission spectrum. The relative fluxes of the emission lines are determined by the shape and strength of the exciting radiation field and the H$_2$ abundances in the rovibrational levels of the ground electronic state. The level populations are determined by the H$_2$ column density and excitation temperature. We computed fluorescence models for a range of excitation temperatures [40 K $\leq T(\mathrm{H}_2) \leq 2000$ K] and column densities [$10^{16} \leq N(\mathrm{H}_2) \leq 2 \times 10^{19}$]. The fluorescence code used the 1030–1040 Å O VI + C II stellar emission model, described above, as the exciting radiation field.

At excitation temperatures ≤ 700 K, fluorescent emission lines excited by absorption out of the $v = 0$ and $J = 0$, 1, and 2 levels dominate the output in the 1100–1187 Å wavelength range. These lines are not seen in the *FUSE* spectra. The observed $(1-3)$ and $(1-4)$ emission lines become the strongest at temperatures above 800 K, providing a lower limit on the excitation temperature. This spectral variation with excitation temperature is due to the distribution of higher rovibrational levels within the ground electronic state. Once the excitation temperature is high enough to significantly populate the $(v, J) = (1, 3)$ level, this fluorescent route dominates due to the coincidence with O VI $\lambda 1032$. An upper limit on $T(\mathrm{H}_2)$ can also be set from the observed spectral characteristics. The lack of Lyα pumped fluorescence indicates (§ 4.2) that the region producing H$_2$ line emission is cooler than ≈ 2000 K.

In order to present a fiducial column density value that gives a sense of the measurement errors, we adopted $T(\mathrm{H}_2) = 1000$ K as a characteristic temperature, which gives a total $N(\mathrm{H}_2) = 4.24^{+2.46}_{-1.82} \times 10^{16}$ cm^{-2}. We emphasize, however, that [$T(\mathrm{H}_2)$,
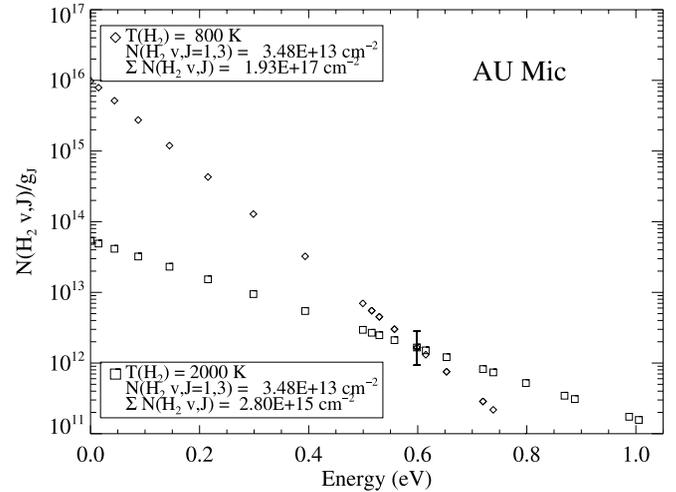
FIG. 3.—H$_2$ column density distributions for $T(\mathrm{H}_2) = 800$ (*diamonds*) and 2000 K (*squares*). Excitation temperatures below 800 K are inconsistent with the observed fluorescent spectrum. Temperatures greater than 2000 K are ruled out by the absence of H$_2$ emission lines pumped by Lyα. Error bars on the column density are shown for the $(v, J) = (1, 3)$ level.

$N(\mathrm{H}_2)$] combinations ranging from [800 K, 1.93×10^{17} cm^{-2}] to [2000 K, 2.80×10^{15} cm^{-2}] are consistent with the data (see § 4.2 for a more detailed discussion of the molecular gas temperature). Column density distributions are shown in Figure 3 for the 800 and 2000 K cases.

4. PHYSICAL PROPERTIES OF THE MOLECULAR GAS COMPONENT

4.1. Mass

A dust mass (M_d) of 0.011 $M_\oplus$ in the AU Mic disk (at $d \leq 70$ AU) was measured by Liu et al. (2004) using 850 μm SCUBA observations. More recently, the dust mass in the AU Mic disk has been estimated from the visible and near-IR scattered light profiles of the disk. Calculations based on scattered light find masses smaller than (about a few to 70×10^{-4} $M_\oplus$ depending on the grain properties and size distribution; Augereau & Beust 2006) or equal to (~ 0.01 $M_\oplus$; Strubbe & Chiang 2006) the submillimeter value. In order to directly compare with H$_2$ absorption studies (Roberge et al. 2005), we use 0.011 $M_\oplus$ as the CS dust mass here. Liu et al. (2004) also set an upper limit on the CO column density in the disk of $N(\mathrm{CO}) \leq 6.3 \times 10^{13}$ cm^{-2} from a CO (3–2) 346 GHz emission nondetection. Assuming an $N(\mathrm{CO})/N(\mathrm{H}_2)$ ratio of 10^{-7}, they place an upper limit on the H$_2$ column in the disk of $N(\mathrm{H}_2) \leq 6.3 \times 10^{20}$ cm^{-2}. Their assumption is supported by recent studies of the diffuse interstellar medium at comparable values of $N(\mathrm{CO})$ where the $N(\mathrm{CO})/N(\mathrm{H}_2)$ ratio is observed to be in the range of a few $\times 10^{-7}$ (Burgh et al. 2007). Liu et al. (2004) place an upper limit on the mass of H$_2$ gas in the disk of $M_{\mathrm{H}_2} \leq 1.3$ $M_\oplus$ and the H$_2$-to-dust ratio in the disk at $M_{\mathrm{H}_2}/M_d \leq 118 : 1$. The limit on this ratio was further decreased by H$_2$ absorption line spectroscopy [Roberge et al. 2005; $N(\mathrm{H}_2) \leq 1.7 \times 10^{19}$ cm^{-2}] to $M_{\mathrm{H}_2}/M_d \leq 6 : 1$.

In comparing the result derived in § 3.2 with that of Liu et al. (2004) we infer values for $N(\mathrm{H}_2)$ that are $\approx 3.3 \times 10^3$ to 2.3×10^5 below their upper limit. The corresponding H$_2$-to-dust ratios are $M_{\mathrm{H}_2}/M_d = [(0.036-5.2) \times 10^{-4}] : 1$, or $M_{\mathrm{H}_2}/M_d \lesssim \frac{1}{30} : 1$. This gives a total mass range of $M(\mathrm{H}_2) = 4.0 \times 10^{-4}$ to 5.8×10^{-6} $M_\oplus$. The value for $T(\mathrm{H}_2) = 1000$ K is $M(\mathrm{H}_2) = 8.7^{+5.2}_{-3.7} \times 10^{-5}$ $M_\oplus$. These results are summarized in Table 2.

$M(H_2)$ $(M_\oplus)$	Technique	M_d^a $(M_\oplus)$	H_2-to-Dust Ratio	Reference
≤ 1.3	CO (3−2) emission	0.011	$\leq 118:1$	Liu et al. (2004)
≤ 0.07	H_2 UV absorption	0.011	$\leq 6:1$	Roberge et al. (2005)
4.0×10^{-4}	H_2 fluorescence	0.011	$0.036:1$	This work, $T(H_2) = 800$ K
5.8×10^{-6}	H_2 fluorescence	0.011	$5.2 \times 10^{-4}:1$	This work, $T(H_2) = 2000$ K

[a] From 850 μm dust emission (Liu et al. 2004).

4.2. *Temperature*

Observations of H_2 emission excited by Lyα through the $B−X$ (1−2) $P(5)$ $\lambda 1216.07$ Å and $B−X$ (1−2) $R(6)$ $\lambda 1215.73$ Å coincidences are generally thought to indicate an H_2 ground-state population characterized by temperatures $T(H_2) > 2000$ K (Black & van Dishoeck 1987; Wood & Karovska 2004; Herczeg et al. 2004; Lupu et al. 2006). In the case where O VI and Lyα excitation are both observed, Lyα excitation usually dominates (e.g., T Tauri stars; Wilkinson et al. 2002; Herczeg et al. 2005). The observation of O VI pumped fluorescence in conjunction with the absence of Lyα fluorescence allows us to constrain the molecular gas temperature in the AU Mic disk. As discussed in § 3.2, the observed fluorescence spectrum sets the lower limit on $T(H_2) \geq 800$ K, and we suggest that the lack of Lyα pumped lines in the *FUSE* data imply an upper limit of $T(H_2) < 2000$ K.

A quantitative calculation of the expected flux from Lyα induced fluorescence is complicated by strong interstellar H I absorption of the line profile (Pagano et al. 2000; Redfield et al. 2002). It seems clear that the local AU Mic Lyα radiation field is at least an order of magnitude more intense than the local O VI radiation field (Fig. 5 in both Pagano et al. [2000] and Redfield et al. [2002]). The A-values for the strongest Lyα pumped lines are similar (to within 30%) to those pumped by O VI (Abgrall et al. 1993a, 1993b). If we ignore optical depth and extinction effects, then the column densities in the absorbing transitions control the resulting emission spectrum. We can define the ratio of column densities in the relevant states, $R_{Ly\alpha}^{O\,VI} \equiv N(1,3)/[N(2,5) + N(2,6)]$. When $R_{Ly\alpha}^{O\,VI} \lesssim 10$ (this value is set by the rough estimate of the stellar Lyα−to−O VI ratio), we would expect a detectable contribution from Lyα pumped fluorescence. For gas temperatures of $T(H_2) = [1000, 2000, 3000, 4000$ K], the corresponding ratios are $R_{Ly\alpha}^{O\,VI} = [545.4, 16.0, 4.9, 2.7]$. Thus, only when $T(H_2) < 2000$ K do we expect to detect H_2 emission from O VI excitation in the absence of lines excited by Lyα.

4.3. *Spatial Origin and Heating*

The H_2 required to produce the observed fluorescence need not be coincident with the stellar line of sight. The emitting gas could reside in a cloud that extends beyond the disk. If the necessary column density suggests absorption that is not observed along the line of sight, this could be evidence for an extraplanar gas component. In order to explore this possibility, we compared a model of the O VI line profile modified by the required H_2 absorption to the O VI profile observed in the *FUSE* spectra (shown in Fig. 4). This assumes that the total required absorbing column density lies along the line of sight, as it would if the H_2 gas is entirely in the disk. The O VI model with the required H_2 absorption superimposed is consistent with the data, within the measurement uncertainties. This leaves open the possibility that all of the emitting H_2 gas lies in the disk, and only the relatively small absorbing column density and low signal-to-noise ratio of the *FUSE* spectra prevent it from being clearly detected in absorp-

tion against the O VI 1032 emission line, as has been observed in other CS disks (Roberge et al. 2001). It is interesting to note that the column density range we derive here [$N(H_2) = 1.9 \times 10^{17}$ to 2.8×10^{15} cm^{-2}] is consistent with the possible line-of-sight absorption suggested in § 4.2 of Roberge et al. (2005).

We can also test whether our $T(H_2)$ estimate is consistent with a disk origin for the emitting gas. A temperature of $T(H_2) \sim 1000$ K is warmer than typical debris disk gas temperatures considered in previous theoretical ($T \leq 300$ K; Kamp & van Zadelhoff 2001) and observational ($T \sim 40$ K [Liu et al. 2004], ≤ 200 K [Roberge et al. 2005]) studies. The first possibility is that the gas is in close proximity to the star. Calculations have been presented for the detectability of Lyα pumped H_2 in the spectra of late-type stars by Jordan et al. (1978), but as we have shown, the temperature of the molecular gas associated with AU Mic is below the level required for that process. Starspots have lower effective temperatures than the conventional photosphere, and the AU Mic spot temperature has been measured in variability studies (Rodono et al. 1986). However, the observed spot temperature, $T_{spot} = 2650$ K, is still substantially above our 2000 K limit. The ratio of spot-to-unspotted temperatures in AU Mic is ~ 0.76. This value agrees well with the spot-to-unspotted temperature ratios found for more massive active stars ($\sim 0.66−0.86$; Neff et al. 1995; O'Neal et al. 1996) from an analysis of TiO absorption bands. We find that even in the coolest regions of the AU Mic surface, a photospheric origin for the observed H_2 emission can most likely be ruled out.

The AU Mic corona is characterized by electron temperatures in the range of 10^4 K $\leq T_e \leq 10^7$ K (Maran et al. 1994). Electron densities in the transition region and coronal regime are of the
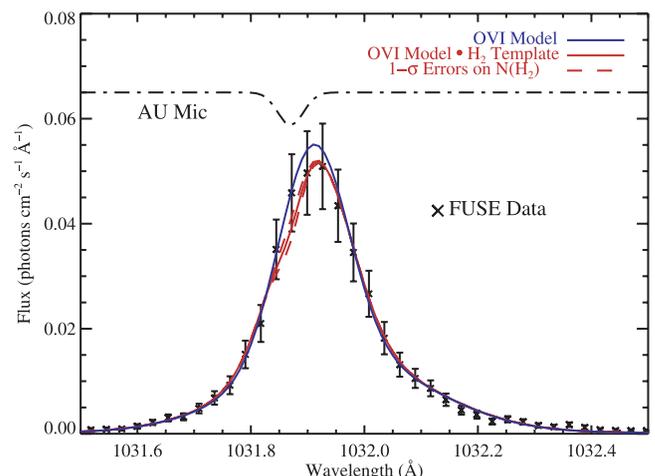
FIG. 4.—Comparison between the predicted and observed O VI line profiles. The blue and red lines are the same as in Fig. 2. The *FUSE* data are overplotted with crosses. The required H_2 absorption is consistent with the observed line profile, within the measurement errors. This indicates that the H_2 absorption could arise completely within the AU Mic CS disk.

order of $n_e = 5 \times 10^{10}$ cm^{-3} (Maran et al. 1994), with suggestions of values several orders of magnitude greater (Redfield et al. 2002). We can estimate the characteristic survival time for molecules near the AU Mic transition and coronal regions by assuming that the H$_2$ is at low densities (i.e., not contained in dense clumps), using $e^- + H_2$ cross sections to determine the collisional dissociation rate (Martin et al. 1998). We take a conservative value for the electron temperature (10^4 K) and find the e-folding time for H$_2$ dissociation via electron impact, $\tau_{\rm diss} = (\gamma_e n_e)^{-1}$, where γ_e is the electron impact dissociation rate coefficient, to be $\tau_{\rm diss} \leq 1$ minute. It is possible that the interstellar conditions assumed to estimate this timescale do not apply directly to the AU Mic environment; however, the basic picture that molecules cannot survive in the immediate environment of AU Mic seems robust even if the parameters vary by several orders of magnitude. As an additional constraint, we consider the possible observational consequences by assuming that molecules could survive in regions as close as a few stellar radii. H$_2$ heated by e^- collisions in the stellar atmosphere might be expected to show the well-characterized signature of electron-impact induced excitation (Ajello et al. 1982, 1984). The electron-impact excitation spectrum of H$_2$ peaks in the *FUSE* and STIS bandpasses (Gustin et al. 2004, 2006), and no emission from these features is observed.

Some grain species may be resistant to sublimation at $r < 6R_*$ (Mann et al. 2006), and it may be possible that the H$_2$ is heated by collisions with grains in thermal equilibrium with the stellar radiation field ($r \approx 6R_*$ for $T = 1000$ K). However, previous studies have found no dust emission or scattered light in the inner disk near AU Mic. In the optical, the disk is cleared inside $r \leq 7.5$ AU (Krist et al. 2005). After probing the 850 μm dust emission, an inner radius of $r \leq 17$ AU is inferred (Liu et al. 2004).

The inferred range of $T(H_2)$ could also be produced by heating processes operating in the disk. There have been considerable efforts toward modeling the gas and dust components of CS disks (Kamp & van Zadelhoff 2001; Jonkheid et al. 2004; Besla & Wu 2007 and references therein), although most of these efforts have focused on higher mass stars (Herbig Ae and T Tauri stars). Nevertheless, we use these models to understand the important processes heating the molecular gas in AU Mic, noting where certain assumptions are invalid for an M star disk. Heating processes include photoelectric heating by grains, collisional de-excitation of H$_2$, photodissociation of H$_2$, H$_2$ formation, gas-grain collisions, carbon ionization, gas-grain drift, and cosmic-ray heating (Kamp & van Zadelhoff 2001). Relevant cooling processes that regulate the gas temperature include [O I] cooling (from 6300 Å and 63.2 μm), [C I] and [C II] cooling, H$_2$ rovibrational line cooling, Lyα cooling, and CO cooling (Kamp & van Zadelhoff 2001).

Gas-grain collisions only heat the gas when $T_{\rm gas} < T_{\rm dust}$, and there is uncertainty whether gas-grain drift is an efficient heating mechanism (Besla & Wu 2007). The gas temperature would have to be much higher than we observe for Lyα or [O I] λ6300 cooling to contribute significantly, and the lifetimes of the rovibrational states of H$_2$ are very long, making these IR transitions inefficient coolants. CO emission is not detected (Liu et al. 2004), so it is hard to assess this contribution to the cooling. Finally, AU Mic lacks the far-UV (912–1110 Å) stellar continuum that drives the photodissociation of H$_2$ and CO, and produces C II through the photoionization of carbon. Processes that depend on this flux (heating: photodissociation of H$_2$ and carbon ionization; cooling: [C II] emission) must be driven solely by the interstellar radiation field (Draine 1978). we presume these processes are of diminished importance in AU Mic relative to models of A star disks.

This leaves photoelectric and H$_2$ formation heating and far-IR fine-structure line cooling as the dominant processes that determine the gas temperature in the AU Mic disk. This conclusion generally agrees with the scenario put forth by Besla & Wu (2007), who calculate gas temperatures in the disks of more massive stars (K2 and earlier) of $T_{\rm gas} > 400$ K, depending on the model parameters. Jonkheid et al. (2004) find that strong photoelectric heating leads to gas temperatures as high as 1000 K in the surface regions of disks, although they consider more strongly flared disks than AU Mic. We note that 1000 K is similar to the temperature found for interstellar H$_2$ where grain-formation pumping is thought to be a dominant excitation source (Spitzer & Cochran 1973). Suffice to say, photoelectric and H$_2$ formation heating seem to be capable of elevating the gas temperature to roughly the observed level, but more modeling work is needed for disks around low-mass stars. We combine this with the arguments against a stellar origin for the observed H$_2$ emission given above, favoring the hypothesis that the fluorescent emission originates in the CS disk.

5. COMPARISON WITH β PIC

AU Mic is a member of the β Pictoris moving group (Zuckerman et al. 2001), meaning the AU Mic disk is roughly the same age as the well-studied β Pic debris disk. The star β Pic (A5 V) is roughly 3.6 times more massive than AU Mic (Kalas et al. 2004). In this section, we briefly compare the molecular gas properties derived for AU Mic with previous observations of gas in the β Pic CS disk.

Multiwavelength model fits to the β Pic CS disk spectral energy distribution predict a dust mass of 0.037 $M_\oplus$ (Dent et al. 2000). The molecular hydrogen mass in β Pic is less clearly defined. *ISO* observations of the mid-IR emission lines of H$_2$ find a large molecular gas reservoir [$M(H_2) \approx 57 M_\oplus$] associated with β Pic (Thi et al. 2001). It seems unlikely that this emission is distributed uniformly throughout the disk. Using UV absorption techniques analogous to those presented for AU Mic (Roberge et al. 2005), Lecavelier des Etangs et al. (2001) report a nondetection of H$_2$ absorption in the edge-on disk. They set an upper limit on the H$_2$ column density of $N(H_2) \leq 10^{18}$ cm^{-2}, corresponding to a molecular gas mass of $\leq 0.095 M_\oplus$.

The ratio of the β Pic and AU Mic dust masses ($\sim$3.4) is approximately equal to the ratio of their stellar masses ($\sim$3.6). The observed dust in both disks is thought to be continually replenished. Collisions of larger parent bodies in the disk can repopulate the small grain population that is detected as scattered light in the optical/near-IR and as thermal emission at longer wavelengths. Models have shown that this scenario can reproduce the observed dust properties of β Pic (Thébault et al. 2003) and AU Mic (Augereau & Beust 2006; Strubbe & Chiang 2006). Grain collisions may also be responsible for replenishing the metallic gas observed in the β Pic disk (Fernández et al. 2006), but it is unclear whether this process contributes to the gas phase H$_2$ abundance.

The H$_2$-to-dust ratio in the β Pic disk (from the UV absorption line upper limit) is $<3:1$. This is consistent with our range of H$_2$-to-dust ratios for AU Mic [$(0.036$–$5.2) \times 10^{-4}:1$]. If H$_2$ gas is present in the β Pic disk at a gas-to-dust ratio similar to that in AU Mic, a natural question arises: Why were the fluorescent emission lines not detected in *FUSE* observations of β Pic? The answer is most likely related to the earlier spectral type of β Pic. The stellar O VI emission line from an active M star such as AU Mic is considerably stronger than in β Pic. The peak flux at the O VI λ1032 line center (coincident with the absorbing H$_2$ transition studied here) is over an order of magnitude higher in AU Mic.

TABLE 3
PREDICTED NEAR- AND MID-IR H$_2$ AU MIC EMISSION LINE BRIGHTNESSES

Line $(v'-v'')\ S(J)$	Wavelength (μm)	Instrument	Brightness[a] (ergs cm^{-2} s^{-1} sr^{-1})
(1–0) $S(1)$	2.12	*HST* NICMOS/ground	9.01×10^{-7}
(2–1) $S(1)$	2.25	Ground	1.13×10^{-9} to 7.47×10^{-8}
(0–0) $S(7)$	5.51	*Spitzer* IRS	5.74×10^{-7} to 4.93×10^{-7}
(0–0) $S(6)$	6.11	*Spitzer* IRS	2.95×10^{-7} to 1.48×10^{-7}
(0–0) $S(5)$	6.91	*Spitzer* IRS	2.02×10^{-6} to 3.30×10^{-7}
(0–0) $S(4)$	8.03	*Spitzer* IRS/ground	8.84×10^{-7} to 6.40×10^{-8}
(0–0) $S(3)$	9.66	*Spitzer* IRS	2.29×10^{-6} to 8.13×10^{-8}
(0–0) $S(2)$	12.28	*Spitzer* IRS/ground	3.84×10^{-7} to 7.39×10^{-9}
(0–0) $S(1)$	17.03	*Spitzer* IRS/ground	2.55×10^{-7} to 2.99×10^{-9}
(0–0) $S(0)$	28.22	*Spitzer* IRS	4.25×10^{-9} to 3.41×10^{-11}

[a] Predicted brightness ranges reflect the adopted temperature ranges of $T(H_2) = 800–2000$ K, corresponding to $N(H_2) = 1.9 \times 10^{17}$ to 2.8×10^{15} cm^{-2}, described in § 3.2.

In addition, the stellar continuum of β Pic extends down to 1100 Å (Lecavelier des Etangs et al. 2001), lowering the line-to-continuum ratio at the strongest emission line wavelengths.

6. IR BRIGHTNESS PREDICTIONS

H$_2$ does not have an intrinsic dipole moment, hence the rovibrational transitions of the molecule proceed by the slower quadrupole channel, making them optically thin in most astrophysical environments (Black & van Dishoeck 1987). Assuming the optically thin case, we used the derived column density distributions ($[T(H_2), N(H_2)] = [800$ K, 1.93×10^{17} cm$^{-2}]$–$[2000$ K, 2.80×10^{15} cm$^{-2}]$) to predict the near and mid-IR H$_2$ emission line strengths for transitions that are observable from ground-based facilities (Speck et al. 2003; Allers et al. 2005), *HST* NICMOS (Meixner et al. 2005), or *Spitzer* IRS (Houck et al. 2004; Hora et al. 2006). The most readily observable H$_2$ lines are the rovibrational lines (1–0) $S(1)$ $\lambda 2.12$ μm and (2–1) $S(1)$ $\lambda 2.25$ μm, and the pure rotational lines (0–0) $S(7)$–$S(0)$ $\lambda\lambda 5$–29 μm. The predicted line intensity can be calculated from

$$I_{mS(J'')} = \left[\frac{N_{p(J''+2)} A_q}{\lambda_q} \right] \frac{hc}{4\pi}, \qquad (2)$$

where $I_{mS(J'')}$ is in units of ergs s^{-1} cm^{-2} sr^{-1} (Black & van Dishoeck 1987; Rosenthal et al. 2000), m is the $(v'-v'')$ transition, p refers to the upper vibrational level, and q labels the A-value and wavelength for the relevant transition. The $J'' + 2$ notation is a consequence of the S branch ($\Delta J = +2$) transition. The A-values are from Wolniewicz et al. (1998). The predicted line strengths are given in Table 3.

The exact detection limits of these lines will be determined by the angular size of the AU Mic emission; a larger filling fraction will increase the observed signal at a given surface brightness. The *Spitzer* IRS has access to the largest number of these lines. Even assuming optimistic aperture filling fractions of unity, the brightest of these lines are predicted to have $F_\nu < 0.05$ mJy, which is at or below the IRS noise limit. This result is consistent with the nondetection of H$_2$ emission from the 15 CS disks around young Sun-like stars in the Formation and Evolution of Planetary Systems *Spitzer* Legacy Program (Pascucci et al. 2006). *HST* NICMOS has the capability for narrowband imaging in the (1–0) $S(1)$ $\lambda 2.12$ μm line, but we predict that achieving contrast with the stellar emission in this bright star ($m_V = 8.8$; Kalas et al. 2004) will be difficult. At a temperature of $T_{eff} = 3500$ K, the photosphere will emit strongly in the near-IR ($\lambda_{max} = 0.83$ μm). Near-IR

imaging will require high dynamic range in flux to achieve contrast between the stellar emission and the faint molecular gas. Calculations for other instruments can be performed using the values in Table 3. We suggest that high-resolution near-IR spectroscopy could be the most promising technique for future observations of H$_2$ in the disk.

7. SUMMARY

We have presented far-UV observations of H$_2$ emission in the AU Microscopii circumstellar disk. The spectra displayed fluorescent emission lines excited by stellar O VI $\lambda 1032$ photons coincident with the $C–X (1–1)\ Q(3)$ $\lambda 1031.87$ Å transition. These lines imply a total column density in the molecular gas of $N(H_2) = 1.9 \times 10^{17}$ to 2.8×10^{15} cm^{-2}. This detection is roughly 2 orders of magnitude smaller than published upper limits on $N(H_2)$. Comparing this value with previous limits on the gas mass in the system, we find $M(H_2) = 4.0 \times 10^{-4}$ to $5.8 \times 10^{-6} M_\oplus$. Using the molecular mass and the 850 μm dust emission, we found a gas-to-dust ratio of $\lesssim \frac{1}{30} : 1$. The derived column densities and gas masses depend on the assumed excitation temperature, which we estimate to be 800–2000 K. We present the basis for this temperature distribution and discuss the value in the context of the AU Mic system. We conclude that the warm H$_2$ is most likely associated with the disk, with photoelectric heating and formation pumping as the dominant heating mechanisms. The intensity was predicted for several near- and mid-IR lines of H$_2$. These lines are accessible to current ground and space-based observatories, although due to the low column density and weak intrinsic nature of the lines, they will be challenging to detect.

Facilities: FUSE, HST

REFERENCES

Abgrall, H., Roueff, E., Launay, F., Roncin, J. Y., & Subtil, J. L. 1993a, A&AS, 101, 273
———. 1993b, A&AS, 101, 323
Ajello, J. M., Shemansky, D., Kwok, T. L., & Yung, Y. L. 1984, Phys. Rev. A, 29, 636
Ajello, J. M., Srivastava, S. K., & Yung, Y. L. 1982, Phys. Rev. A, 25, 2485
Allers, K. N., Jaffe, D. T., Lacy, J. H., Draine, B. T., & Richter, M. J. 2005, ApJ, 630, 368
Augereau, J.-C., & Beust, H. 2006, A&A, 455, 987
Bally, J., Testi, L., Sargent, A., & Carlstrom, J. 1998, AJ, 116, 854
Besla, G., & Wu, Y. 2007, ApJ, 655, 528
Black, J. H., & van Dishoeck, E. F. 1987, ApJ, 322, 412
Burgh, E. B., France, K., & McCandliss, S. R. 2007, ApJ, 658, 446
Dent, W. R. F., Walker, H. J., Holland, W. S., & Greaves, J. S. 2000, MNRAS, 314, 702
Draine, B. T. 1978, ApJS, 36, 595
Feldman, P. D., Weaver, H. A., & Burgh, E. B. 2002, ApJ, 576, L91
Fernández, R., Brandeker, A., & Wu, Y. 2006, ApJ, 643, 509
France, K. 2005, Ph.D. thesis, Johns Hopkins Univ.
France, K., Andersson, B.-G., McCandliss, S. R., & Feldman, P. D. 2005, ApJ, 628, 750
Gustin, J., Cowley, S. W. H., Gérard, J.-C., Gladstone, G. R., Grodent, D., & Clarke, J. T. 2006, J. Geophys. Res. Space Phys., 111, 9220
Gustin, J., et al. 2004, Icarus, 171, 336
Haisch, K. E., Jr., Lada, E. A., & Lada, C. J. 2001, ApJ, 553, L153
Herczeg, G. J., Linsky, J. L., Walter, F. M., Gahm, G. F., & Johns-Krull, C. M. 2006, ApJS, 165, 256
Herczeg, G. J., Wood, B. E., Linsky, J. L., Valenti, J. A., & Johns-Krull, C. M. 2004, ApJ, 607, 369
Herczeg, G. J., et al. 2005, AJ, 129, 2777
Hora, J. L., Latter, W. B., Smith, H. A., & Marengo, M. 2006, ApJ, 652, 426
Houck, J. R., et al. 2004, ApJS, 154, 18
Hubickyj, O., Bodenheimer, P., & Lissauer, J. J. 2005, Icarus, 179, 415
Jonkheid, B., Faas, F. G. A., van Zadelhoff, G.-J., & van Dishoeck, E. F. 2004, A&A, 428, 511
Jordan, C., Brueckner, G. E., Bartoe, J.-D. F., Sandlin, G. D., & van Hoosier, M. E. 1977, Nature, 270, 326
———. 1978, ApJ, 226, 687
Kalas, P., Liu, M. C., & Matthews, B. C. 2004, Science, 303, 1990
Kamp, I., & van Zadelhoff, G.-J. 2001, A&A, 373, 641
Krist, J. E., et al. 2005, AJ, 129, 1008
Laughlin, G., Bodenheimer, P., & Adams, F. C. 2004, ApJ, 612, L73
Lecavelier des Etangs, A., et al. 2001, Nature, 412, 706

Linsky, J. L., & Wood, B. E. 1994, ApJ, 430, 342
Liu, M. C., Matthews, B. C., Williams, J. P., & Kalas, P. G. 2004, ApJ, 608, 526
Liu, W., & Dalgarno, A. 1996, ApJ, 462, 502
Lupu, R. E., France, K., & McCandliss, S. R. 2006, ApJ, 644, 981
Mann, I., Köhler, M., Kimura, H., Cechowski, A., & Minato, T. 2006, A&A Rev., 13, 159
Maran, S. P., et al. 1994, ApJ, 421, 800
Martin, P. G., Keogh, W. J., & Mandy, M. E. 1998, ApJ, 499, 793
McCandliss, S. R. 2003, PASP, 115, 651
Meixner, M., McCullough, P., Hartman, J., Son, M., & Speck, A. 2005, AJ, 130, 1784
Moos, H. W., et al. 2000, ApJ, 538, L1
Neff, J. E., O'Neal, D., & Saar, S. H. 1995, ApJ, 452, 879
O'Neal, D., Saar, S. H., & Neff, J. E. 1996, ApJ, 463, 766
Pagano, I., Linsky, J. L., Carkner, L., Robinson, R. D., Woodgate, B., & Timothy, G. 2000, ApJ, 532, 497
Pascucci, I., et al. 2006, ApJ, 651, 1177
Redfield, S., Ayres, T. R., Linsky, J. L., Ake, T. B., Dupree, A. K., Robinson, R. D., & Young, P. R. 2003, ApJ, 585, 993
Redfield, S., Linsky, J. L., Ake, T. B., Ayres, T. R., Dupree, A. K., Robinson, R. D., Wood, B. E., & Young, P. R. 2002, ApJ, 581, 626
Roberge, A., Feldman, P. D., Lagrange, A. M., Vidal-Madjar, A., Ferlet, R., Jolly, A., Lemaire, J. L., & Rostas, F. 2000, ApJ, 538, 904
Roberge, A., Weinberger, A. J., Redfield, S., & Feldman, P. D. 2005, ApJ, 626, L105
Roberge, A., et al. 2001, ApJ, 551, L97
Rodono, M., et al. 1986, A&A, 165, 135
Rosenthal, D., Bertoldi, F., & Drapatz, S. 2000, A&A, 356, 705
Sahnow, D. J., et al. 2000, ApJ, 538, L7
Shull, J. M. 1978, ApJ, 224, 841
Shull, M., & Beckwith, S. 1982, ARA&A, 20, 163
Speck, A. K., Meixner, M., Jacoby, G. H., & Knezek, P. M. 2003, PASP, 115, 170
Spitzer, L. J., & Cochran, W. D. 1973, ApJ, 186, L23
Strubbe, L. E., & Chiang, E. I. 2006, ApJ, 648, 652
Thébault, P., Augereau, J. C., & Beust, H. 2003, A&A, 408, 775
Thi, W. F., et al. 2001, ApJ, 561, 1074
Valenti, J. A., Johns-Krull, C. M., & Linsky, J. L. 2000, ApJS, 129, 399
Wilkinson, E., Harper, G. M., Brown, A., & Herczeg, G. J. 2002, AJ, 124, 1077
Wolniewicz, L., Simbotin, I., & Dalgarno, A. 1998, ApJS, 115, 293
Wood, B. E., & Karovska, M. 2004, ApJ, 601, 502
Wood, B. E., Linsky, J. L., & Ayres, T. R. 1997, ApJ, 478, 745
Zuckerman, B., Song, I., Bessell, M. S., & Webb, R. A. 2001, ApJ, 562, L87